Collisional Activation of Small Peptides

Oussama Meroueh and William L. Hase*

Department of Chemistry, Wayne State University, Detroit, Michigan 48202

Received: December 10, 1998; In Final Form: March 17, 1999

Classical trajectory simulations are performed to study the efficiency of energy transfer in the collisional activation of polyglycine and polyalanine peptide ions with β-sheet and α-helix structures. Energy-transfer efficiencies for collisions with Ar are determined versus impact parameter, peptide size and structure, mass of the collider, the collision energy, and the form of the intermolecular potential between the peptide and argon. High-level ab initio calculations, for Ar interacting with small molecules representing the peptides' functional groups, are performed to determine an accurate Ar + peptide intermolecular potential. Energy transfer may be efficient and in some cases as high as 80%. There is a low collision energy regime in which the percent energy transfer increases as the peptide size increases. However, at higher energies, an apparent impulsive energy-transfer regime is reached where the peptide size has a negligible effect on the energy-transfer efficiency. For a certain peptide size, structure may have a significant effect on energy transfer; i.e., α-helix peptide structures tend to be activated more efficiently than are β-sheet structures. Heavy rare-gas atoms such as Kr and Xe are much more efficient collision activators than a light collider like He. The form of the collision's repulsive intermolecular potential has a strong influence on the energy-transfer efficiency. Collisional energy transfer to peptide rotational energy is not insignificant and at high collision impact parameters may surpass energy transfer to peptide vibration. For many of the trajectories there are multiple encounters between the collider and peptide during a collision.

I. Introduction

Recent methods[1] for desorbing and ionizing peptides in the gas phase have made it possible to carry out extensive collision-induced dissociation (CID) mass spectrometry studies[2−8] on these molecules. In a typical experiment of this type, the peptide is vibrationally excited through a series of collisions with a bath gas and undergoes unimolecular dissociation when its internal vibrational energy exceeds the dissociation limit. Because of the size and complexity of the peptides, the activation dynamics, which lead to specific dissociation mechanisms, have been difficult to characterize. Several factors are thought to be involved in the energy transfer and collisional activation. They include the collision impact parameter, the size of the peptide ion, the mass of the bath gas, the center-of-mass collision energy, and the folding pattern (i.e., structure) of the peptide.

Several theoretical studies have been done to elucidate the fragmentation mechanism of large peptides. Vékey et al.[9] have used semiempirical and ab initio methods to obtain bond order and potential energy profiles of single- and double-protonated tetraglycine. These calculations have provided some insight on how protonation of the nitrogen atom instead of the carboxyl oxygen affects the peptide's fragmentation pattern. Their results support earlier calculations done by Somogyi et al.,[10] which showed that protonation of the amide bond nitrogen rather than the carboxyl oxygen enhances weakening of the amide bond. Other methods[11] include the use of RRKM theory to qualitatively understand the energetics associated with peptide dissociation.

Classical trajectory simulations make it possible to study collision processes in detail. Simulations of collisional energy transfer from highly excited polyatomics have been performed for a number of molecules including benzene,[12] toluene,[13] SF_6,[14] azulene,[15] and stillbene.[16] Classical trajectory simulations have also been used to study the collisional activation of large biological molecules.[4,8,17] These studies have considered model peptide intramolecular potentials[17] and model peptide−bath gas intermolecular potentials[4,8,17] and have not attempted to average all impact parameters and peptide orientations contributing to the collisional activation. However, these simulations have revealed that a substantial fraction of the collision energy may be transferred to internal modes of the peptide.[4,8,17] Multiple encounters between the bath-gas collider and individual atoms of the peptide, during the collision event, facilitate energy transfer.[8] Trajectory simulations have also provided insight into the CID of metal atom clusters.[18−21]

As a result of the high collision energy and the large density of internal vibrational/rotational states for the peptide, classical trajectories are expected to accurately model peptide collisional excitation.[22] In the work presented here, classical trajectory simulations of argon colliding with protonated polyglycine and polyalanine peptides are used to determine dynamical attributes of the collisional activation. The effects of impact parameter and size of the peptide on the energy transfer are studied at different fixed translational energies. Since a peptide may exist in a number of different folded and unfolded structures, how the compactness of the peptide structure affects energy transfer is also studied.

II. Computational Details

A. Potential Energy Function. The general analytic potential energy function used for the Ar−peptide systems is represented as

$$V = V_{\text{peptide}} + V_{\text{Ar, peptide}} \tag{1}$$

when V_{peptide} is the protonated peptide intramolecular potential and $V_{\text{Ar,peptide}}$ is the Ar−peptide intermolecular potential. The

10.1021/jp984712b CCC: $18.00
Published on Web 04/29/1999

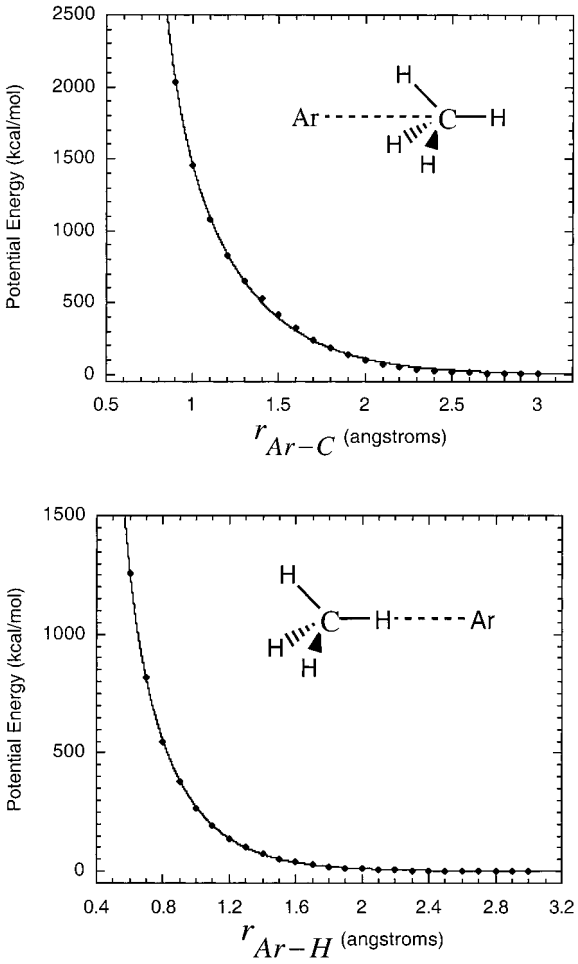

Figure 1. Ab initio and fitted, eq 3, potential energy curves for Ar + CH_4.

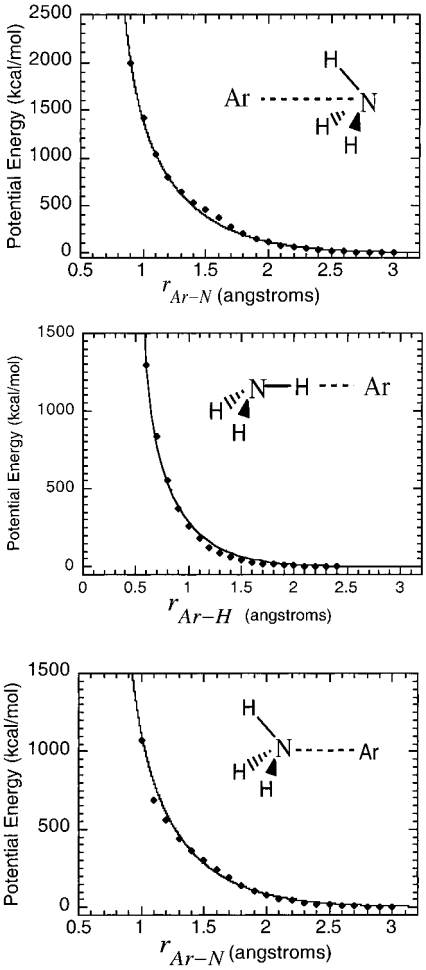

Figure 2. Ab initio and fitted, eq 3, potential energy curves for Ar + NH_3.

former is the Amber valence force field of Cornell et al.[23] and is expressed as

$$V_{\text{peptide}} = \sum_{\text{bonds}} K_r(r - r_{\text{eq}})^2 + \sum_{\text{angles}} K_\theta(\theta - \theta_{\text{eq}})^2 + \sum_{\text{dihedrals}} \frac{V_n}{2}[1 - \cos(n\phi - \gamma)] + \sum_{i>j}[A_{ij}/r_{ij}^{12} - B_{ij}/r_{ij}^{6} + q_i q_j/(\epsilon r_{ij})] \quad (2)$$

Protonated polyglycine and polyalanine peptides are studied here and are identified as $(\text{gly})_n$ and $(\text{ala})_n$.

Trajectory simulations of metal atom cluster CID have shown that the efficiency of collisional energy transfer is strongly dependent on the repulsiveness of the intermolecular potential,[19−21] so considerable care was taken to derive an accurate Ar−peptide intermolecular potential. This was done by using ab initio calculations at the QCISD(T)/6-31++G** level of theory[24] to calculate intermolecular potentials between Ar and small molecules representative of peptide functional groups, from which two-body interaction potentials of the form

$$V(r) = a\, e^{-br} + \frac{c}{r^9} \quad (3)$$

were derived to represent repulsive interactions between Ar and each atom type of the peptide. Since high-energy collisions are considered in this work, no attempt was made to fit the shallow potential energy minima between Ar and the model molecules. The counterpoise method[25,26] was used to correct the ab initio results for basis set superposition error. The inner electrons are important for the short-range repulsive potentials calculated here. Thus, in contrast to the long-range attractive potentials, the short-range potentials are less sensitive to the detailed electronic structure for each atom. The CH_4, NH_3, NH_4^+, and H_2CO molecules are expected to represent the short-range repulsive interactions for the polyglycines and polyalanines studied here.

The interaction potentials between Ar and an H atom attached to a C atom and between Ar and an sp^3 C atom were obtained by performing ab initio calculations for Ar interacting with CH_4 along the Ar···H−C and H−C···Ar C_{3v} axes. The resulting ab initio energy curves are plotted in Figure 1. The potentials between Ar and the N and H atoms of an amine group were determined from Ar/NH_3 ab initio calculations, which are shown in Figure 2. The potential curves are for Ar interacting with NH_3 front-side and back-side, along the C_{3v} axis, and interacting along an N−H bond.

Since the N-terminal amine group has the highest proton affinity in the absence of basic side chains,[27] the proton is assumed to be attached to the end nitrogen, and thus, the interaction between argon and the atoms of the protonated amine end group was modeled by interactions of the argon atom with an ammonium molecule. As for the above Ar/CH_4 ab initio calculations, Ar/NH_4^+ interactions were calculated for both front-side and back-side C_{3v} interactions. The ab initio curves are plotted in Figure 3. The two-body interaction potentials between Ar and the atoms of a carboxylic group were

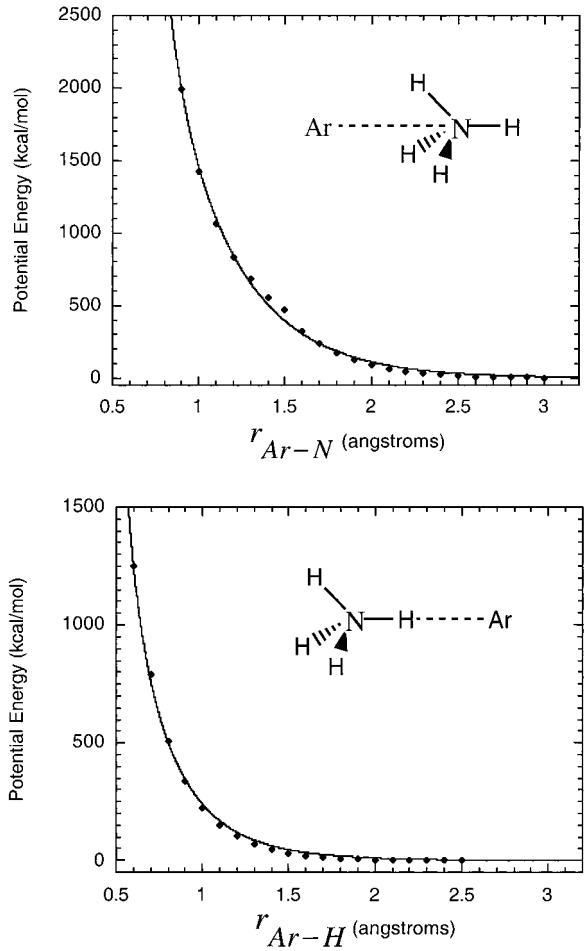

Figure 3. Ab initio and fitted, eq 3, potential energy curves for Ar + NH_4^+.

determined from four sets of ab initio calculations for the Ar/formic acid system. Intermolecular potentials were calculated for interactions along the O−H···Ar, C═O···Ar, and Ar···C═O axes and for Ar interacting with the O atom of OH along an Ar···O axis parallel to the C═O bond (see Figure 4). The potential energy curves for these four calculations are given in Figure 4.

TABLE 1: Intermolecular Potential Parameters[a]

potential	*a*	*b*	*c*
Ar/CH_4(ArC)	11202.65	2.399515	152.7291
Ar/CH_4(ArH)	8668.195	3.801426	1.727232
Ar/NH_3(ArN)	8186.600	2.328971	218.8906
Ar/NH_3(ArH)	4220.855	2.982401	3.719138
Ar/NH_4^+(ArN)	13609.85	2.433643	101.5290
Ar/NH_4^+(ArH)	10803.06	4.406716	2.066664
Ar/HCO_2H(ArOH)[b]	15387.06	2.698321	90.09528
Ar/HCO_2H(ArHO)	8696.623	4.196012	5.277458
Ar/HCO_2H(ArCO)	8471.329	4.648228	304.6066
Ar/HCO_2H(ArOC)	12914.72	2.681826	99.56698

[a] Parameters for eq 3 with *a*, *b*, and *c* in units of kcal/mol, $Å^{-1}$, and kcal $Å^9$/mol, respectively. [b] Two-body potential between Ar and an oxygen atom of the OH group of a carboxylic acid group.

The parameters for eq 3 were obtained by simultaneously fitting all the potential energy curves for each system studied. The resulting fits are plotted in Figures 1−4, and it is seen that there is excellent agreement between the ab initio and fitted curves. The potential parameters derived for the two-body potentials are listed in Table 1.

B. Peptide Equilibrium Structures. Initial conditions for the protonated polyglycine and polyalamine peptides were chosen by adding a quasiclassical 300 K Boltzmann distribution of vibrational/rotational energies (see below) to a potential energy minimum of the peptide. In this presentation, these protonated peptides are identified by $(gly)_n$ and $(ala)_n$. To compare the energy transfer dynamics of different size peptides with the same common structure, the potential minima for extended β-sheet structures of $(gly)_n$ and $(ala)_n$ were studied. The structures for these $(gly)_n$ peptides are shown in Figure 5. The β-sheet $(ala)_n$ structures are similar, except an H atom of each amino acid is replaced by a CH_3 group. Calculations were also performed with the folded α-helix structures of the $(ala)_n$

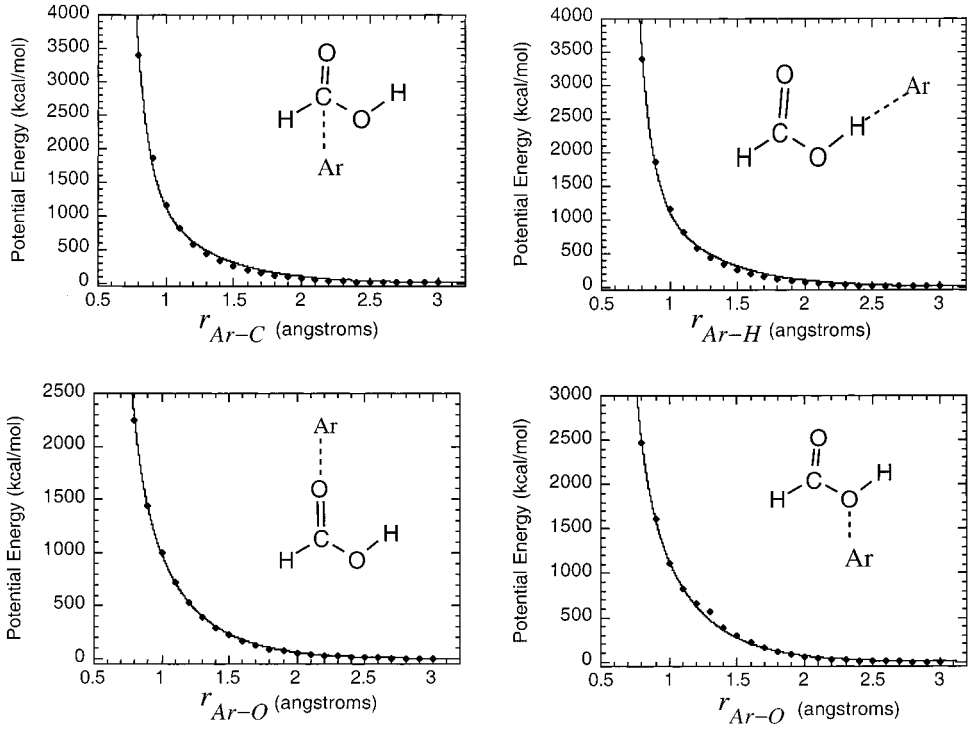

Figure 4. Ab initio and fitted, eq 3, potential energy curves for Ar + H_2CO_2.

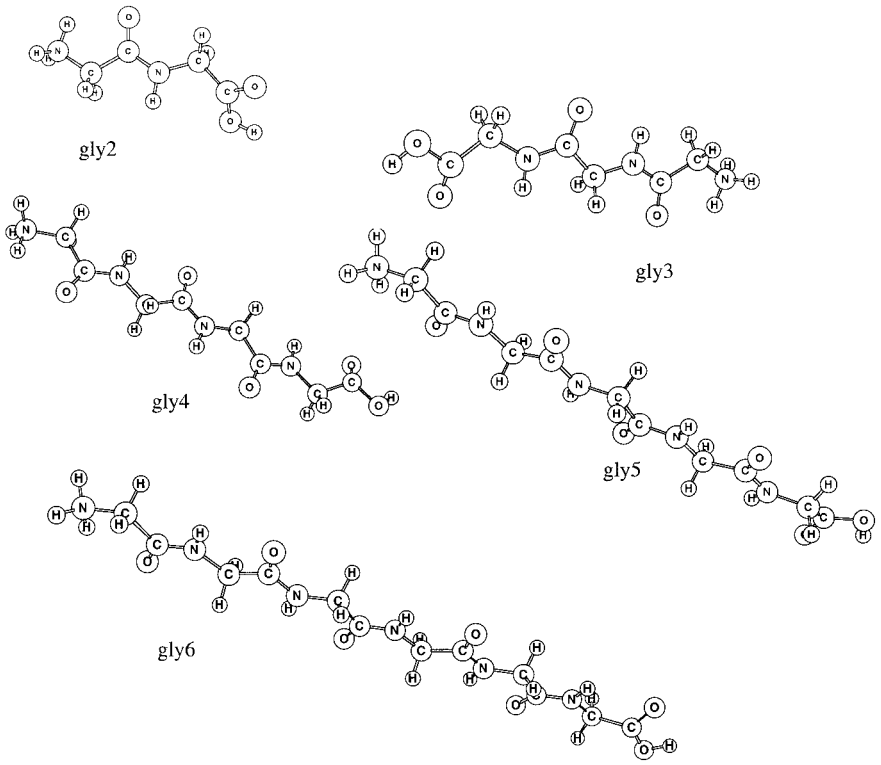

Figure 5. Polyglycine extended β-sheet structures used for the energy-transfer simulations.

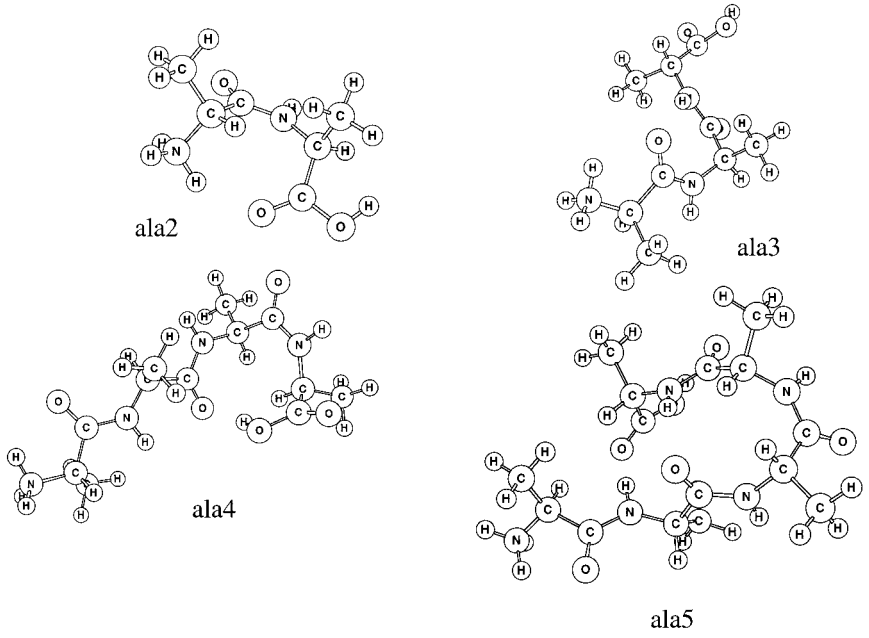

Figure 6. Polyalanine folded α-helix structures used for the energy-transfer simulations.

peptides (see Figure 6) to study how the structure of the peptide affects energy transfer. Additional studies of this effect were made by performing simulations with different initial structures of $(gly)_4$. A range of folded and extended structures were determined for $(gly)_4$ by running trajectories at 3000 K and then quenching the trajectories at random time intervals into the different potential minima they accessed. The different structures investigated for $(gly)_4$ are shown in Figure 7. In the following, the β-sheet structures in Figure 5 are identified by β, and the α-helix structures in Figure 6 are identified by an α.

C. Trajectory Simulations. The classical trajectories[28−32] were calculated with the general chemical dynamics computer program VENUS96.[33] Both the analytic potential energy functions described above and the method described below for selecting initial momenta and coordinates for the Ar + peptide collision are standard options in VENUS96.

The quasiclassical normal mode method[34−36] was used to select initial coordinates and momenta for the peptide. Energies for the peptide's normal modes of vibration were selected from a 300 K Boltzmann distribution.[36] The energy for each normal mode was partitioned between kinetic and potential by choosing a random phase for the normal mode.[34] A 300 K rotational energy of $RT/2$ was added to each principal axis of rotation of the peptide. The algorithms for transforming these vibrational and rotational energies to Cartesian momenta and coordinates have been described previously.[34,35] The peptide was then

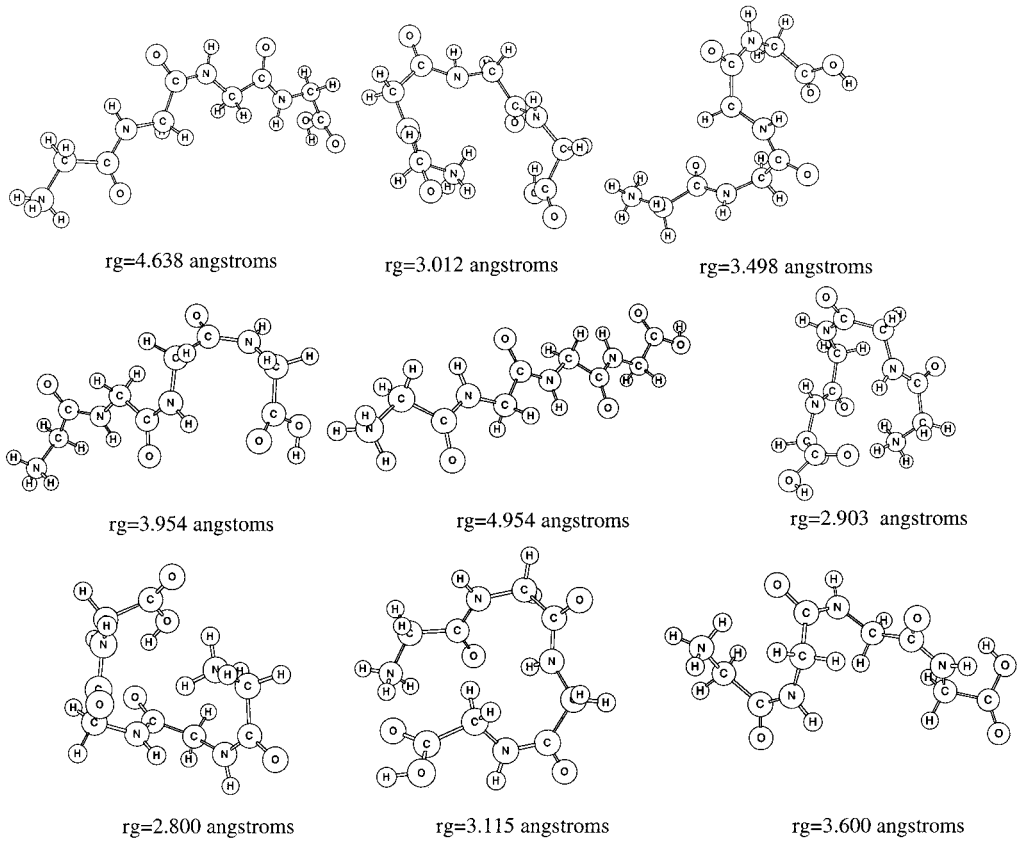

Figure 7. Structures of $(gly)_4$ investigated for energy-transfer efficiency. The radius of gyration is given for each structure.

randomly rotated about its Euler angles.[37] Relative velocities were then added to Ar and the peptide in accord with the center-of-mass collision energy and the collision impact parameter.[37] Collision energies of 100, 500, and 1000 kcal/mol were considered. The impact parameter b was either set to a specified value or chosen randomly between 0 and b_{max}. The criterion for selecting the maximum impact parameter b_{max} is described in the results section.

VENUS96 uses a combined Runge−Kutta and Adams−Moulton algorithm to propagate the trajectories. The integration time step was chosen to be 0.06 fs, small enough so that energy is conserved to seven significant figures. Trajectories are initiated and stopped at distances large enough to guarantee no interaction between the peptide and the argon atom. The property determined from the trajectories is the amount of relative translational energy transferred to the peptide. To study the dynamics of this energy-transfer process, the relative translational energy, the energy of the peptide, and the peptide structure were analyzed as a function of time. Uncertainties in the reported results are the standard deviation in the mean,[38] which is the standard deviation divided by the square root of the total number of trajectories. Five hundred trajectories were calculated for each initial condition studied unless otherwise stated.

III. Energy-Transfer Efficiency

A. Effect of Collision Impact Parameter. To determine the role of the impact parameter, the average energy transfer versus impact parameter $\langle \Delta E(b) \rangle$ was calculated for Ar collisions with the β-$(gly)_n$, $n = 2-7$, peptides for an initial relative translational energy $E_{rel} = 100$ kcal/mol. Figure 8 shows the results of these calculations. As one would expect, the average fraction of energy transfer decreases with an increase in impact parameter, with the most rapid decline for the smallest peptide. At $b = 0$ the peptides have average energy transfer efficiencies in the range ∼50−60%. The largest b at which measurable energy transfer occurs varies from 7 to 16 Å in going from β-$(gly)_2$ to β-$(gly)_7$.

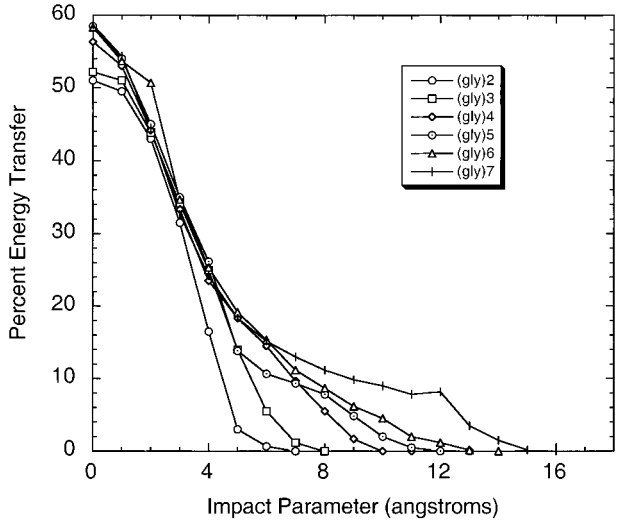

Figure 8. Percent energy transfer to β-$(gly)_n$ structures vs impact parameter at $E_{rel} = 100$ kcal/mol.

Obtaining a value for an average energy transfer per collision by considering all collisional impact parameters requires the definition of a maximum impact parameter b_{max}. Since the classical collision cross section is infinite for the long-range r^{-9} potential in eq 3, because of a finite energy transfer for all impact parameters, unambiguously defining b_{max} remains a difficult problem. However, several operative approaches have been proposed for choosing b_{max}.[38−40] A quantity that may be converged from the trajectory simulations is the average energy transfer versus impact parameter $\langle \Delta E(b) \rangle$ integrated over the

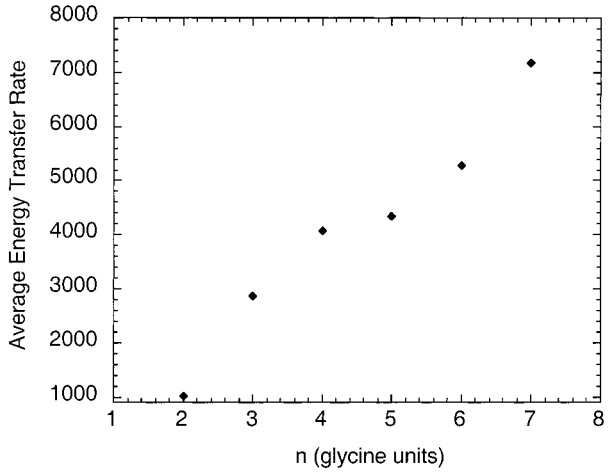

Figure 9. $\langle \Delta E \rangle_\sigma$ from eq 4 vs the size of the β-sheet polyglycine. $\langle \Delta E \rangle_\sigma$ has units of kcal Å^2/mol.

differential collision cross section $2\pi b\ \mathrm{d}b$;[41] i.e.,

$$\langle \Delta E \rangle_\sigma = \int_0^\infty \langle \Delta E(b) \rangle 2\pi b\ \mathrm{d}b \tag{4}$$

Values for $\langle \Delta E \rangle_\sigma$ versus the size of the β-(gly)$_n$ peptide are plotted in Figure 9 for $E_{rel} = 100$ kcal/mol. $\langle \Delta E \rangle_\sigma$ increases nearly linearly from 1000 kcal Å^2/mol for β-(gly)$_2$ to 7169 kcal Å^2/mol for β-(gly)$_7$.

A value for $\langle \Delta E \rangle$, averaged over b, may be determined by dividing $\langle \Delta E \rangle_\sigma$ by the collision cross section πb_{max}^2. Values for b_{max} were deduced from eq 4 by setting the integral's upper limit to the value of b, which gives a $\langle \Delta E \rangle_\sigma$ value within 10^{-4} % of the limiting value. Nearly identical values for b_{max} are attained by using a fitting criteria of 1 or 1×10^{-2} %. The resulting b_{max} values for β-(gly)$_n$ are 7.0, 7.6, 10.2, 11.7, 13.2, and 15.4 Å for $n = 2$, 3, 4, 5, 6, and 7, respectively. These b_{max} values are similar to those one would deduce visually from Figure 8. Using these values for b_{max} and the values in Figure 9 for $\langle \Delta E \rangle_\sigma$ gives $\langle \Delta E \rangle$ of 13.1, 15.8, 12.4, 10.1, 9.7, and 9.7 kcal/mol for $n = 2$, 3, 4, 5, 6, and 7, respectively. These values tend to slightly decrease with increase in peptide size.

Figure 10 gives the energy transfer distributions for Ar collisions with β-(gly)$_4$ and β-(gly)$_6$ for $E_{rel} = 100$ kcal/mol and b chosen randomly between 0 and b_{max}. The distributions are broad and show that most if not all of the collision energy is accessible for conversion into peptide internal energy. The large elastic peak results from the fact that for some impact parameters less than b_{max} the peptide is oriented so that Ar and the peptide do not strongly interact. This is a result of the extended, unfolded structures for the peptide. A smaller elastic peak would be expected for a folded, more spherical peptide structure (see below).

B. Effect of Peptide Size. Early studies[42] of the effect of molecular size on the energy-transfer process for organic cyclic molecules indicated that the average energy transfer per collision decreases with increasing molecular size. More recently, low-energy CID experiments on a homologous series of *n*-alkylbenzenes were carried out by Nacson et al.[43] The size of the ions was increased by gradually increasing the alkyl chain length. By comparing product ratios from CID data to energy-resolved electron impact data, Nacson et al. found that the maximum internal energy deposited into the ion increases with alkyl chain length.

CID experiments performed on peptides[44,45] have shown increasing difficulty in enhancing fragmentation as the size of the peptide is increased. However, recently, Marzluff et al.[4] have performed CID experiments on a series of peptides and have found that greater dissociation occurs as the peptide becomes larger.

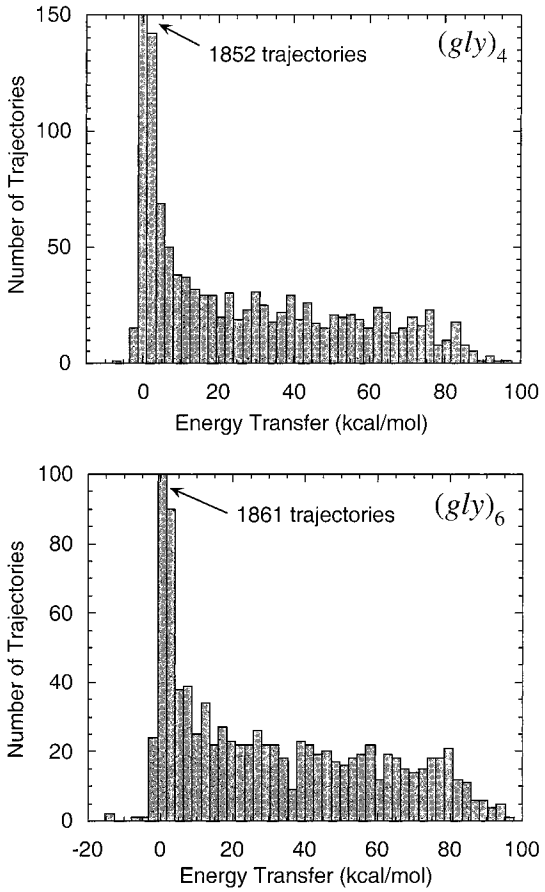

Figure 10. Energy-transfer distributions for collisions of Ar with β-sheet (gly)$_4$ and (gly)$_6$ with $E_{rel} = 100$ kcal/mol and b chosen randomly between zero and b_{max}. b_{max} equals 10.3 and 13.2 Å for (gly)$_4$ and (gly)$_6$, respectively. Two thousand seven hundred fifty trajectories were calculated for each distribution. The elastic energy-transfer peak for (gly)$_4$ and (gly)$_6$ contains 1852 and 1861 events, respectively.

The calculations discussed above show that for Ar collisions with polyglycines at $E_{rel} = 100$ kcal/mol, the average energy transfer $\langle \Delta E \rangle$ averaged over the impact parameter is rather insensitive to the size of the peptide. To study in more detail the effect of peptide size on the collisional activation, the average energy transfer was obtained for the collision of Ar with both polyglycines and polyalanines for E_{rel} values of 100, 500, and 1000 kcal/mol. Extended β-sheet structures were considered for the polyglycines, while these structures as well as folded, α-helix structures were considered for the polyalanines (see Figures 5 and 6). To circumvent the need to choose a value for b_{max} and to consider the ambiguity in the large elastic peak in the energy-transfer distribution, these trajectory simulations were performed for $b = 0$. These calculations allow comparisons in the energy-transfer efficiency as a function of peptide size and collision energy.

The results of the above simulations are shown in Figure 11. At $E_{rel} = 100$ kcal/mol there is a linear-like increase in the percent energy transfer versus the polypeptide's number of atoms. For β-(gly)$_n$ and α-(ala)$_n$ peptides with the same number of atoms, the energy-transfer efficiencies are very similar. The β-(ala)$_n$ peptides have somewhat smaller energy transfers. Different energy transfer patterns are observed at E_{rel} of 500 and 1000 kcal/mol compared to the $E_{rel} = 100$ kcal/mol results. At

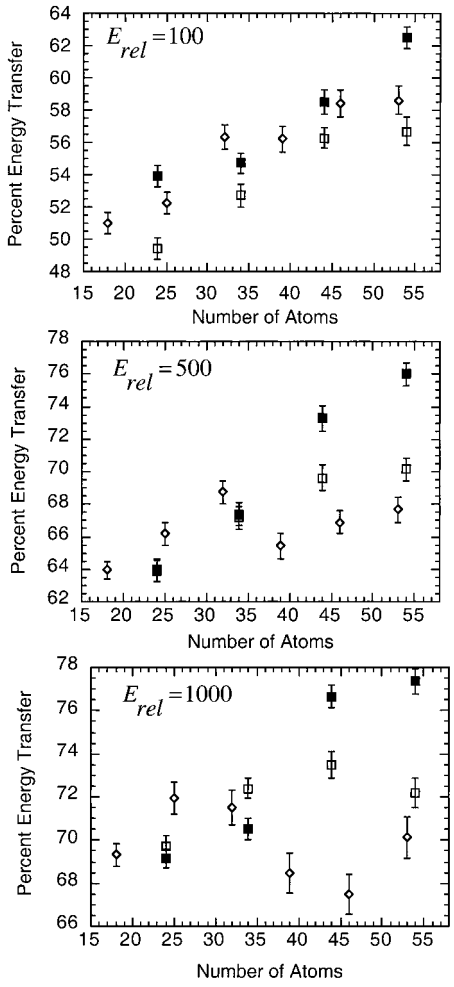

Figure 11. Percent energy transfer at $b = 0$ vs size of $(gly)_n$ and $(ala)_n$ polypeptides for E_{rel} of 100, 500, and 1000 kcal/mol: (■) α-$(ala)_n$; (□) β-$(ala)_n$; (◇) β-$(gly)_n$.

these higher E_{rel}, the percent energy transfer to the different size β-sheet peptides shows no apparent trend, with a variation of only 4%. On the other hand, the percent energy transfer increases nearly linearly, i.e., by 12% at 500 kcal/mol and 8% at 1000 kcal/mol, as the α-$(ala)_n$ size increases from n of 2 to n of 5.

C. Effect of Peptide Structure. The above results for the β-sheet and α-helix polyalanines show that the efficiency of energy transfer depends on the peptide's structure. This property was considered in more detail by investigating collisions with different structures of the $(gly)_4$ peptides. The specific structures of these peptides are given in Figure 7.

The results of $b = 0$ collisions, with the $(gly)_4$ peptides at $E_{rel} = 100$ and 1000 kcal/mol, are given in Figure 12 versus the peptide's radius of gyration r_g, which is defined as

$$r_g = \left(\frac{\sum r_i^2}{n+1}\right)^{1/2} \tag{5}$$

where the r_i are the distances of the n atoms from the peptide's center of mass. Figure 12 shows that even though the collisions are head-on with $b = 0$, the structure of the peptide affects the efficiency of energy transfer. For the collisions at $E_{rel} = 100$ kcal/mol, there is a near-linear 15% decrease in the percent energy transfer as r_g increases from 3 to 5 Å. Though such a linear trend is not seen at $E_{rel} = 1000$ kcal/mol, there is still a predominant decrease in the energy-transfer efficiency as r_g is increased. The general result from these calculations is that the more compact, folded structures give the most efficient energy transfer.

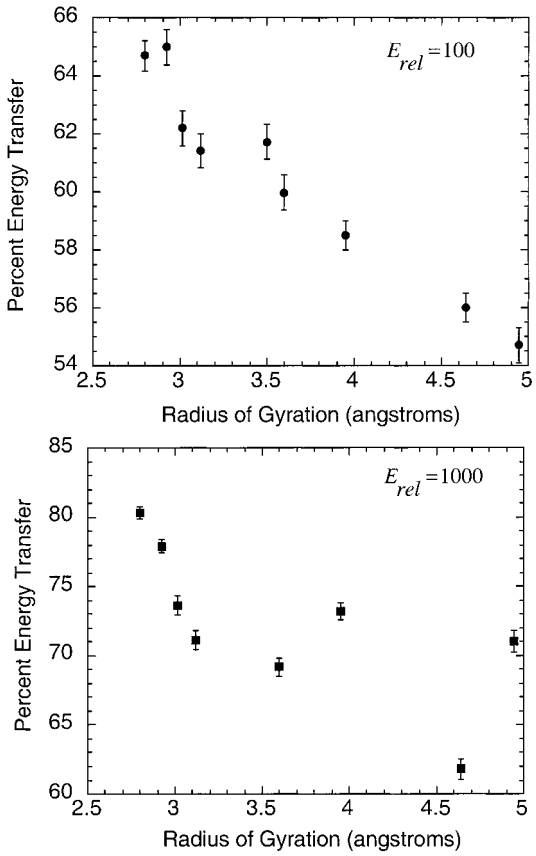

Figure 12. Percent energy transfer at $b = 0$ and $E_{rel} = 100$ and 1000 kcal/mol for the $(gly)_4$ structures in Figure 7.

D. Effect of the Ar−Peptide Intermolecular Potential. As discussed above, high-level ab initio calculations were performed to determine an accurate potential energy function for the Ar−peptide intermolecular interactions. It is of interest to determine the sensitivity of the energy-transfer results to the form of this potential and to determine how the results change if a less accurate, purely empirical potential is used. A potential of this type was created from experimental Ar−Ar Lennard-Jones parameters[46] and Lennard-Jones parameters for H, C, N, and O in different bonding environments from the potential of Cornell et al.[23] The Lorentz−Berthelot combinations rules[47] were used to construct two-body potentials of the form

$$V_{Ar,i} = \frac{A_{Ar,i}}{(r_{Ar,i})^{12}} - \frac{B_{Ar,i}}{(r_{Ar,i})^6} \tag{6}$$

where

$$A_{Ar,i} = \sqrt{\epsilon_{Ar}\epsilon_i}(R_{Ar,i})^{12}$$
$$B_{Ar,i} = 2\sqrt{\epsilon_{Ar}\epsilon_i}(R_{Ar,i})^6 \tag{7}$$

and i denotes an atom on the peptide, the ϵ's are Lennard-Jones well depths, and the $R_{Ar,i}$ are the sum of the radii for the Ar and i-atom Lennard-Jones minima. The resulting A and B values for the Ar/N, Ar/C−H, Ar/C═O, Ar/O═C, Ar/H−N, Ar/H−C, Ar/H−O, and Ar/O−H interactions are, respectively, 1 466 387, 1135.672; 1 539 574, 1042.247; 1 365 027, 924.0840; 950 358.8, 963.8619; 3616.949, 31.092 98; 98 789.73, 162.4976; 0.00, 0.00; 1 162 981, 1066.753. The first value in each pair is A in kcal Å^{12}/mol, and the second is B in kcal Å^6/mol.

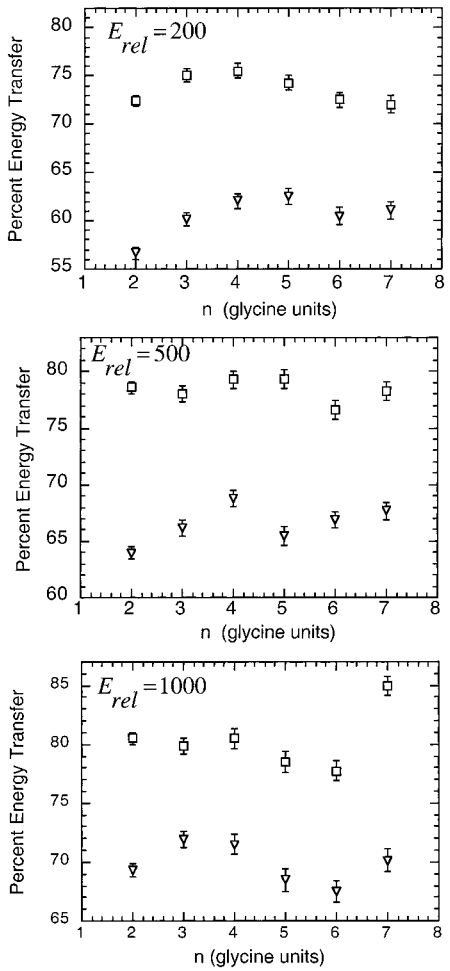

Figure 13. Comparison of energy-transfer efficiencies for Ar + β-(gly)$_n$ collisions, determined with the ab initio potential (▽), eq 3, and model empirical potential (□), eq 7. The impact parameter is zero. E_{rel} is in kcal/mol.

A comparison of results for Ar collisions with β-(gly)$_n$ peptides, obtained with this potential and the above ab initio potential, is given in Figure 13. The two potentials give significantly different energy-transfer efficiencies, with the percent energy transfer as much as 30% larger for the empirical Lennard-Jones potential. This difference between these two sets of results points out the need for using an accurate intermolecular potential. As shown below in section IV, the different energy-transfer efficiencies for the two potentials are explained by their range parameters. One similarity between the results of the two potentials is that both predict a small increase in the energy transfer efficiency as E_{rel} is increased.

E. Times for Ar + Peptide Encounters. Times for Ar + peptides encounters, with an initial zero impact parameter, were determined from plots of the vibrational/rotational internal energy of the peptides as a function time. This analysis was performed for 10 randomly chosen trajectories for each of the following systems: β-(gly)$_4$ at E_{rel} = 100 kcal/mol; β-(gly)$_7$ at E_{rel} = 100 kcal/mol; α-(ala)$_5$ at E_{rel} of 100 and 1000 kcal/mol. Typical results are shown in Figure 14 for Ar + α-(ala)$_5$ collisions at E_{rel} = 100 kcal/mol. One of the collisions is direct, with only one encounter between Ar and the peptide. However, the other is indirect with multiple encounters, identified by sharp changes in the slope of the peptide's energy versus time. The direct collision has an encounter time of ∼100 fs, while the indirect collision with multiple encounters has a total encounter time of ∼180 fs.

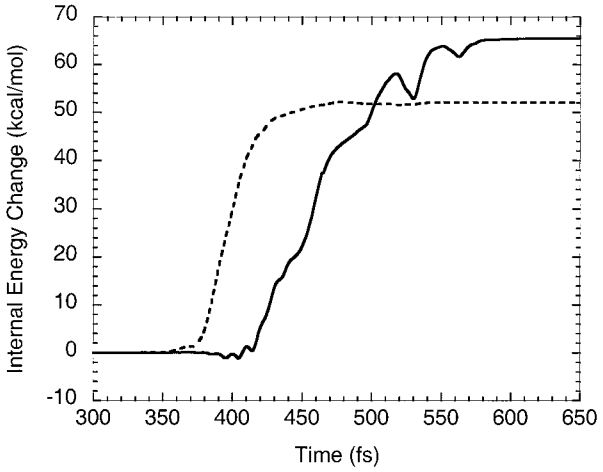

Figure 14. Example of a direct trajectory and indirect trajectory with multiple encounters for the Ar + α-(ala)$_5$ system at E_{rel} = 100 kcal/mol.

The relative number of trajectories with a direct encounter, two encounters, and multiple encounters was 1:3:6 for the Ar + β-(gly)$_4$ system at E_{rel} = 100 kcal/mol. The encounter time ranged between 70 and 135 fs, with an average value of 100 fs. For the Ar + β-(gly)$_7$ system's 10 trajectories at E_{rel} = 100 kcal/mol, the average encounter time was 145 fs, with a range of 55−300 fs. The relative number of these trajectories with a direct encounter, two encounters, and multiple encounters was 4:1:5. For the Ar + α-(ala)$_5$ system, the distribution of the 10 trajectories between a direct encounter, two encounters, and multiple encounters was 1:2:7 at 100 kcal/mol and 1:6:3 at 1000 kcal/mol. The average encounter time and range were 180 and 120−250 fs at 100 kcal/mol, and 80 fs and 40−125 fs at 1000 kcal/mol.

Overall, there are no extraordinary differences in the above analyses for β-(gly)$_4$, β-(gly)$_7$, and α-(ala)$_5$. In particular, the results for the β-sheet and α-helix structures at the same E_{rel} of 100 kcal/mol are quite similar. More than 50% of the trajectories for each system have two or more encounters between Ar and the peptide during a collision. This effect will have to be incorporated into any theoretical model describing the efficiency of energy transfer in peptide collisional activation. This incomplete analysis also suggests that the encounter time tends to increase as either the peptide size is increased or E_{rel} is decreased. Both of these findings seem physically correct. As the peptide becomes larger, multiple encounters over a longer period of time are possible. Increasing E_{rel} increases the peptide's velocity and should decrease the time Ar and the peptide are in contact. The results for α-(ala)$_5$ suggest the number of multiple encounters may decrease as E_{rel} as increased. In the future, it will be of interest to probe each of these issues with more complete analyses.

F. Effect of the Collider's Mass. The effect of the collider's mass on the energy-transfer efficiency was investigated by adjusting the Ar mass to values for He, Ne, Kr, and Xe. The intermolecular potential between the collider and the peptide was not varied. The impact parameter was set to zero and E_{rel} values of 100, 500, 1000, 2000, and 4000 kcal/mol were considered. The results for the α-(ala)$_5$ peptide are given in Table 2, where it is seen that the energy-transfer efficiencies are significantly smaller for He and Ne but only slightly larger for Kr and Xe. Energy-transfer efficiencies for β-(ala)$_5$ at E_{rel} of 100 and 1000 kcal/mol are in parentheses in Table 2. They are slightly smaller than those for α-(ala)$_5$.

G. Peptide Vibrational and Rotational Energies. To model the unimolecular dissociation of a collisionally activated peptide,

TABLE 2: Average Percent Energy Transfer for Rare-Gas/α-(ala)$_5$ Collisions[a]

	collision energy (kcal/mol)				
rare gas	100	500	1000	2000	4000
He	35 (29)[b]	36	48 (37)	40	42
Ne	57 (52)	63	74 (66)	69	66
Ar	63 (57)	76	77 (72)	75	70
Kr	66 (63)	74	77 (75)	76	67
Xe	68 (66)	75	80 (74)	74	64

[a] The collision impact parameter is zero. The ab initio Ar + peptide intermolecular potential was used for each rare gas. Five hundred trajectories were calculated for each percent energy transfer. [b] The percent energy transfer for β-(ala)$_5$ peptides is in parentheses.

it is important to know how the collision energy transferred to the peptide is partitioned between vibrational and rotational energy.[48] This property was studied as a function of impact parameter in Ar collisions with β-(gly)$_4$ at E_{rel} = 100 kcal/mol. The resulting values of the $\langle\Delta E_{vib}\rangle$, $\langle\Delta E_{rot}\rangle$ pair in units of kcal/mol for b in the range 1−7 Å are the following: 46.1, 6.9 for 1 Å; 35.2, 9.0 for 2 Å; 22.9, 10.3 for 3 Å; 12.2, 11.4 for 4 Å; 7.2, 11.1 for 5 Å; 5.1, 9.3 for 6 Å; 2.4, 7.3 for 7 Å. The energy transfer is predominantly to peptide vibration and rotation at small and large b, respectively. At b = 4 Å similar amounts of energy are transferred to vibration and rotation. In addition to the impact parameter, the partitioning of the energy transfer between peptide vibration and rotation may also depend on the collision energy and the peptide structure. For example, folded α-helix peptide structures may absorb vibrational energy more efficiently than do the extended, β-sheet structures. Issues such as these are very important for modeling peptide dissociation and will be considered in detail in future work.

IV. Discussion

It is of interest that the refined impulsive translation to vibration (T → V) energy transfer model developed by Mahan[49,50] for collinear A + BC collisions provides a qualitative interpretation of certain aspects of the above results. In this model the fraction of E_{rel} transferred to BC vibration is

$$\Delta E/E_{rel} = 4\cos^2\beta\sin^2\beta\left(\frac{\xi}{2}\operatorname{cosech}\frac{\xi}{2}\right)^2 \qquad (8)$$

where

$$\cos^2\beta = m_A m_C/[(m_A + m_B)(m_B + m_C)] \qquad (9)$$

The ξ term is often called the *adiabaticity* parameter and is given by

$$\xi = 4\pi^2\nu L/v_{rel} \qquad (10)$$

where ν is the BC vibrational frequency, v_{rel} the A + BC initial relative velocity, and L the range parameter for an A−B intermolecular potential of the form $V(r) = V_0\exp(-r/L)$. The energy transfer $\Delta E/E_{rel}$ increases as ξ decreases. When $\xi < 1$ the collisions are in the *sudden* limit, with a very short collision time compared to the vibrational period, and $\Delta E/E_{rel}$ attains its maximum value of 4 $\cos^2\beta\sin^2\beta$. Since the Ar−peptide collisions are not collinear and there is a broad distribution of peptide vibrational frequencies, quantitative agreement with Mahan's model is not expected.

As the size of the (gly)$_n$ or (ala)$_n$ peptide increases, the distribution of vibrational frequencies for the peptides extends to lower values and, in an average sense, ξ decreases for E_{rel} held constant. Thus, if the collisions are not in the sudden limit, more efficient energy transfer is expected as n is increased. This is the behavior observed for both the β-sheet and α-helix peptides at E_{rel} of 100 kcal/mol (see Figure 11). At E_{rel} of 500 and 1000 kcal/mol, the energy transfer results for the β-sheet (ala)$_n$ and (gly)$_n$ peptides are those expected for the sudden limit, where $\Delta E/E_{rel}$ is nearly independent of peptide size and, thus, vibrational frequency. However, at these high energies the percent energy transfer to the α-(ala)$_n$ peptides still increases near-linearly with increasing n. Energy transfer to these α-helix structures attains the sudden limit for even higher E_{rel}. At E_{rel} = 3000 kcal/mol and b = 0, the energy transfer to α-helix (ala)$_2$ and (ala)$_5$ are 67 and 69%, respectively, and are nearly the same.

For the smaller β-sheet peptides with the same number of atoms, energy transfer is more efficient to (gly)$_n$ than (ala)$_n$ (see Figure 11). However, the opposite is found for the larger peptides. These differences cannot be explained by the vibrational frequencies for these two peptides, since (gly)$_n$ and (ala)$_n$ with the same number of atoms have very similar distributions of harmonic vibrational frequencies. The vibrational frequencies also do not explain why a higher E_{rel} is required to attain the sudden limit for the α-helix compared to the β-sheet structures. For the same size peptide the two structures have nearly identical vibrational frequency distributions. This is illustrated by the 0−500 cm^{-1} frequencies for (ala)$_5$. The β-sheet structure has 52 frequencies in this range, with an average value of 204 cm^{-1}, while the α-helix structure has 53 frequencies and an average of 222 cm^{-1}. The dependence of energy transfer on structure extends to low energies. At E_{rel} = 25 kcal/mol and b = 0, the percent energy transfer is 42 and 50 for the (gly)$_7$ and (ala)$_5$ β-sheet structures and 50 for α-(ala)$_5$.

Since peptides with the same vibrational frequencies, mass, and intermolecular potential are predicted to have the same energy efficiency according to Mahan's model, this model does not provide a qualitative interpretation of the above dependence of the energy-transfer efficiency on peptide structure. This is further exemplified by the results in Figure 12 for the different (gly)$_4$ structures. The energy-transfer efficiency to the peptide varies by up to 15% as its structure is changed. This is a very significant result and clearly needs additional investigation. At E_{rel} of 1000 kcal/mol, Figure 12 shows that peptides with much different structures may have similar energy-transfer efficiencies, which suggests some of the peptide structures may have reached the sudden limit.

The manner in which a change in the Ar/peptide intermolecular potential affects energy transfer is qualitatively explained by Mahan's model. Range parameters L for both the ab initio potential, eq 3, and the model intermolecular potential, eq 7, were determined by fitting these potentials to $V(r) = V_0\exp(-r/L)$. The resulting L values are ∼2.5 times larger for the ab initio potential, and as a result, eq 8 predicts less efficient energy transfer for the ab initio potential, as observed in the trajectories (Figure 13). This finding points out the need for accurate intermolecular potentials to calculate meaningful energy-transfer efficiencies.

If m_B in eq 9 is assumed to be the atom or functional group with which atom A collides and if m_C is the mass of the remainder of the peptide and, thus, much larger than either m_A or m_B, the 4 $\cos^2\beta\sin^2\beta$ term in eq 8 becomes $4m_Am_B/(m_A + m_B)$,[2,51] which has its maximum value when $m_A = m_B$. That the percent energy transfer plateaus and does not decrease with increase in m_A (see section III.F) suggest that A does not collide with a single atom of the peptide and that an effective value for m_B varies as m_A is changed. To consider this property in more detail, an impulsive energy-transfer model derived for col-

lisions with macromolecules was used to fit the results in Table 2 for rare-gas atoms colliding with α-$(ala)_5$. This model gives[52]

$$\langle \Delta E \rangle / E_{rel} = \frac{4 m_A m_B (m_A + m_M)(m_M - m_B)}{(m_A + m_B)^2 m_M^2} \qquad (11)$$

where m_M is the peptide mass, which is 374 amu for $(ala)_5$. The fitting parameter is m_B, an effective mass of a moiety with which the rare-gas atom collides. The resulting m_B values increase in going from m_A for He to that for Xe and, except for Xe, are largest at E_{rel} of 100 kcal/mol. The specific m_B values for each rare-gas atom, listed respectively, for E_{rel} of 100, 500, 1000, 2000, and 4000 kcal/mol are the following: He, 34, 33, 23, 29, 27; Ne, 74, 65, 51, 57, 61; Ar, 101, 82, 80, 84, 93; Kr, 155, 135, 128, 128, 130; Xe, 182, 165, 152, 166, 191. For each rare-gas atom the smallest fitted value of m_B is for $E_{rel} = 1000$ kcal/mol. An increase in m_B in going from He to Xe is consistent with the increasing size of the rare-gas atom and the resulting greater number of intermolecular interactions with the atoms of the peptide.

V. Conclusion

The simulations reported here have provided details of how energy transfer in peptide collisional activation is influenced by the peptide size and structure, collision energy, and mass of the collider. The energy-transfer efficiency is strongly dependent on the collider/peptide intermolecular potential and, thus, accurate potentials are required to compare with experimental results. The simulations suggest that there are a variety of collider/peptide collision types, ranging from direct to indirect with multiple collider−peptide encounters. The way in which the collisional activation is distributed between peptide vibrational and rotational energy depends on the collision impact parameter.

The results of this study suggest numerous future areas of study. It would be of interest to determine how the partitioning of the collisional activation between peptide vibration and rotation and the nature of the activating collisions are influenced by the peptide size, structure, and composition. This may provide some insight into how peptide structure affects energy transfer. It would be of interest to include peptides in the 100−1000 atom range in these studies. To more efficiently determine collision times, it would be helpful to have a physical criterion for identifying when the collision begins and ends. Finally, it would be of interest to identify whether there is a particular class (or classes) of peptide vibrational modes that are initial acceptors of energy in the collisional activation.

Acknowledgment. This research was supported by the National Science Foundation.

References and Notes

(1) Orlov, V. M.; Pustogaev, V. N.; Masslova, R. N. *Mol. Biol.* **1996**, *30*, 444.
(2) Johnson, R. S.; Martin, S. A.; Biemann, K. *Int. J. Mass Spectrom. Ion Processes* **1988**, *86*, 137.
(3) Poulter, L.; Taylor, L. C. E. *Int. J. Mass. Spetrom. Ion Processes* **1989**, *91*, 183.
(4) Marzluff, E. M.; Campbell, S.; Rodgers, M. T.; Beauchamp, J. L. *J. Am. Chem. Soc.* **1994**, *116*, 7787.
(5) Doroshenko, V. M.; Cotter, R. J. *Anal. Chem.* **1996**, *68*, 463.
(6) Vachet, R. W.; Winders, A. D.; Glish, G. L. *Anal. Chem.* **1996**, *68*, 522.
(7) Klassen, J. S.; Kerbale, P. *J. Am. Chem. Soc.* **1997**, *119*, 6552.
(8) Marzluff, E. M.; Beauchamp, J. L. In *Large Ions: Their Vaporization, Detection and Structural Analysis*; Baer, T., Ng, C. Y., Powis, I., Eds.; Wiley: New York, 1996; p 115.
(9) Vekey, K.; Gomory, A. *Rapid Commun. Mass Spectrom.* **1990**, *119*, 6552.
(10) Somogyi, A.; Wysocki, V. H.; Mayer, I. *J. Am. Chem. Soc.* **1994**, *5*, 704.
(11) Marzluff, E. M.; Campbell, S.; Rodgers, M. R.; Beauchamp, J. L. *J. Am. Chem. Soc.* **1994**, *116*, 6947.
(12) Lenzer, T.; Luther, K. *Ber. Bunsen-Ges. Phys. Chem.* **1997**, *101*, 581.
(13) Bernshtein, V.; Oref, I. *J. Chem. Phys.* **1996** *104*, 1958.
(14) Lendvay, G.; Schatz, G. C. *J. Chem. Phys.* **1993**, *98*, 1034.
(15) Gilbert, R. G.; Lim, K. F. *J. Phys. Chem.* **1990**, *94*, 78.
(16) Bolton, K.; Nordholm, S. *Chem. Phys.* **1996**, *206*, 103.
(17) Gilbert, R. G.; Sheil, M. M.; Derrick, P. *J. Org. Mass Spectrom.* **1985**, *120*, 430.
(18) Shulte, J.; Lucchese, R. R.; Malow, W. H. *J. Chem. Phys.* **1993**, *99*, 1178.
(19) de Sainte Claire, P.; Peslherbe, G. H.; Hase, W. L. *J. Phys. Chem.* **1995**, *99*, 8147.
(20) de Sainte Claire, P.; Hase, W. L. *J. Phys. Chem.* **1996**, *100*, 8190.
(21) Hase, W. L.; de Sainte Claire, P. In *Highly Excited Molecules. Relaxation, Reaction, and Structure*; Mullin, A. S., Schatz, G. C., Eds.; ACS Symposium Series 678; American Chemical Society: Washington, DC, 1997; Chapter 19.
(22) *Comparisons of Classical and Quantum Dynamics, Advances in Classical Trajectory Methods*; Hase, W. L., Ed.; JAI Press: Greenwich, CT, 1998; Vol. 3.
(23) Cornell, W. D.; Cieplak, P.; Bayley, C. I.; Gould, I. R.; Merz, K. M.; Ferguson, D. M.; Spellmeyer, D. C.; Fox, T.; Caldwell, J. W.; Kollman, P. A. *J. Am. Chem. Soc.* **1995**, *117*, 5179.
(24) Frisch, M. J.; Trucks, G. W.; Schlegel, H. B.; Gill, P. M. W.; Johnson, B. G.; Robb, M. A.; Cheeseman, J. R.; Keith, T.; Petersson, G. A.; Montgomery, J. A.; Raghavachari, K.; Al-Laham, M. A.; Zakrzewski, V. G.; Ortiz, J. V.; Foresman, J. B.; Cioslowski, J.; Stefanov, B. B.; Nanayakkara, A.; Challacombe, M.; Peng, C. Y.; Ayala, P. Y.; Chen, W.; Wong, M. W.; Andres, J. L.; Replogle, E. S.; Gomperts, R.; Martin, R. L.; Fox, D. J.; Binkley, J. S.; Defrees, D. J.; Baker, J.; Stewart, J. P.; Head-Gordon, M.; Gonzales, C.; Pople, J. A. *Gaussian 94*; Gaussian, Inc.: Pittsburgh, PA, 1995.
(25) Boys, S. F.; Bernardi, F. *Mol. Phys.* **1970**, *19*, 553.
(26) Tao, F. M.; Pan, Y. K. *J. Phys. Chem.* **1991**, *95*, 3582.
(27) Morgan, D. G.; Bursey, M. M. *J. Mass Spectrom.* **1995**, *30*, 290.
(28) Bunker, D. L. *Methods Comput. Phys.* **1971**, *10*, 287.
(29) Bunker, D. L. *Acc. Chem. Res.* **1974**, *7*, 195.
(30) Porter, R. N.; Raff, L. M. In *Dynamics of Molecular Collisions, Part B*; Miller, W. H., Ed.; Modern Theoretical Chemistry 2; Plenum: New York, 1976; Chapter 1.
(31) Raff, L. M.; Thompson, D. L. In *Theory of Chemical Reactions Dynamics*; Baer, M., Ed.; Boca Raton, FL, 1985; Vol. III.
(32) Sewell, T. D.; Thompson, D. L. *Int. J. Mod. Phys. B* **1997**, *11*, 1067.
(33) Hase, W. L.; Duchovic, R. J.; Hu, X.; Komornicki, A.; Lim, K. F.; Lu, D.-h.; Peslherbe, G. H.; Swamy, K. N.; Vande Linde, S. R.; Varandas, A.; Wang, H.; Wolf, R. J. *QCPE* **1996**, *16*, 671.
(34) Chapman, S.; Bunker, D. L. *J. Chem. Phys.* **1975**, *62*, 2890.
(35) Sloane, C. S.; Hase, W. L. *J. Chem. Phys.* **1977**, *66*, 1523.
(36) Cho, Y. J.; Vande Linde, S. R.; Zhu, L.; Hase, W. L. *J. Chem. Phys.* **1992**, *96*, 8275.
(37) Hase, W. L.; Ludlow, D. M.; Wolf, R. J.; Schlick, T. *J. Phys. Chem.* **1981**, *85*, 958.
(38) Laitinen, H. A. *Chemical Analysis*; McGraw-Hill: New York, 1960; p 545.
(39) Lendvay, G.; Schatz, G. C. *J. Chem. Phys.* **1992**, *96*, 3752. Hu, X.; Hase, W. L. *J. Phys. Chem.* **1988**, *92*, 4040.
(40) Lim, K. F.; Gilbert, R. G. *J. Phys. Chem.* **1990**, *94*, 72.
(41) Whyte, A. R.; Lim, K. F.; Gilbert, R. G.; Hase, W. L. *Chem. Phys. Lett.* **1988**, *152*, 377.
(42) Carr, R. W. J. *Chem. Phys. Lett.* **1980**, *74*, 437.
(43) Nacson, S.; Harrison, A. G. *Int. J. Mass Spectrom. Ion Processes* **1985**, *63*, 325.
(44) Alexander, A. J.; Thibault, P.; Boyd, R. K.; Curtis, J. M.; Rinehart, K. L. *Int. J. Mass Spectrom. Ion Processes* **1990**, *98*, 107.
(45) Alexander, A. J.; Boyd, R. K. *Int. J. Mass Spectrom. Ion Processes* **1989**, *90*, 211.
(46) Scoles, G. *Annu. Rev. Phys. Chem.* **1980**, *31*, 81.
(47) Hansen, J.-P.; McDonald, I. R. *Theory of Simple Liquids*; Academic: New York, 1986.
(48) Baer, T.; Hase, W. L. *Unimolecular Reaction Dynamics. Theory and Experiments*; Oxford: New York, 1996; pp 224−239.
(49) Mahan, B. H. *J. Chem. Phys.* **1970**, *52*, 5221.
(50) Yardley, J. T. *Introduction to Molecular Energy Transfer*; Academic Press: London; pp 95−129. Shin, H. K. In *Dynamics of Molecular Collisions*; Miller, W. H., Ed.; Plenum: New York, 1976; Part A, Chapter 4.
(51) The same expression is obtained from an impulsive energy-transfer model for macromolecules. Uggerud, E.; Derrick, P. *J. Chem. Phys.* **1991**, *95*, 1430.
(52) Since the trajectories are calculated for $b = 0$, $\langle \Delta E \rangle$ is set equal to ΔE_{max} for the theoretical model of ref 49.